PERGAMON

International Journal of Solids and Structures 38 (2001) 203–225

INTERNATIONAL JOURNAL OF SOLIDS and STRUCTURES

www.elsevier.com/locate/ijsolstr

Effective elastoplastic behavior of metal matrix composites containing randomly located aligned spheroidal Inhomogeneities. Part II: applications

L.Z. Sun [a], J.W. Ju [b,*]

[a] *Department of Civil and Environmental Engineering, and Center for Computer-Aided Design, The University of Iowa, Iowa City, IA 52242-1527, USA*

[b] *Department of Civil and Environmental Engineering, University of California, 5731/5732 Boelter Hall, Los Angeles, CA 90095-1593, USA*

Received 05 August 1998; in revised form 11 January 2000

Abstract

Based on the proposed formulation in Part I of this sequel (Ju, J.W., Sun, L.Z., Int. J. Solids Struct. 38, 183–201), effective elastoplastic constitutive relations are implemented in this article for metal matrix composites (MMCs) with randomly located and unidirectionally aligned spheroidal particles. First, we investigate the uniaxial elastoplastic stress–strain behavior of MMCs. In particular, we perform comparisons among the theoretical uniaxial stress–strain predictions, existing finite element results and experimental data for MMCs to illustrate the capability of the proposed method. Furthermore, the effect of stress triaxiality is discussed under either the purely hydrostatic or axisymmetric loading on the overall elastoplastic behavior of composites. The proposed initial effective yield surfaces for composites are demonstrated and compared with those of the experimental data. As a special case of the incompressible ductile material containing aligned spheroidal voids, the initial effective yield criterion is studied and compared with that of mathematical upper bound. Finally, viscoplastic extension is briefly presented.

Keywords: Micromechanics; Elastoplasticity; Metal-matrix composites; Random microstructure; Spheroidal inhomegeneity

1. Introduction

In Ju and Sun (2000), a novel formulation is proposed to predict the overall elastoplastic behavior of two-phase metal matrix composites (MMCs) containing randomly located and unidirectionally aligned spheroidal inhomogeneities. Local micromechanics is employed to render a new expression for the "exterior-point" Eshelby's tensor (Eshelby, 1957, 1959, 1961; Mura, 1987), which represents the strain and stress influences of an ellipsoidal inhomogeneity upon a material point located within the matrix phase. In particular, explicit tensorial components of both the exterior- and interior-point Eshelby's tensors of a

* Corresponding author. Tel.: +1-310-206-1751; fax: +1-310-267-2283.
E-mail address: juj@ucla.edu (J.W. Ju).

0020-7683/00/$ - see front matter
PII: S0020-7683(00)00026-3

spheroidal inclusion are derived. The ensemble-average homogenization procedure is utilized to derive the overall yield function of particle reinforced MMCs (PRMMCs) based on the probabilistic spatial distribution of aligned spheroidal particles. The overall elastoplastic constitutive equations are characterized for PRMMCs under three-dimensional loading and unloading conditions.

In this study, focus is upon the implementation of the framework proposed in Part I of this sequel. Specifically, the overall uniaxial, purely hydrostatic and axisymmetric elastoplastic stress–strain responses of PRMMCs are investigated. Comparisons of stress–strain curves and initial yield surfaces are performed among our model predictions, experimental data, finite element results, and mathematical bounds for PRMMCs and porous ductile materials to illustrate the capability of the proposed method. Finally, extension to viscoplasticity is briefly presented.

2. Uniaxial stress–strain behavior of PRMMCs

2.1. Governing equations

In material engineering, the uniaxial stress–strain relationship is often referred to as the mechanical behavior of materials. In order to illustrate the micromechanics-based elastoplastic formulation for PRMMCs in Part I of this sequel (Ju and Sun, 2000), it is of interest to consider the case of the uniaxial stress loading. Specifically, the applied macroscopic stress $\bar{\sigma}$ can be written as

$$\bar{\sigma}_{11} > 0, \quad \text{all other } \bar{\sigma}_{ij} = 0. \tag{1}$$

Note that the aligned axisymmetric axis of spheroidal inclusions is denoted as the x_1-axis.

From Eq. (64) in Part I (Ju and Sun, 2000), the macroscopic incremental elastic strain can be derived in terms of the incremental uniaxial stress $\Delta\bar{\sigma}_{11}$ as

$$[\Delta\bar{\epsilon}^{\mathrm{e}}_{ij}] = \begin{bmatrix} D_{11} & 0 & 0 \\ 0 & D_{12} & 0 \\ 0 & 0 & D_{12} \end{bmatrix} \Delta\bar{\sigma}_{11}, \tag{2}$$

where the effective elastic compliance constants read

$$D_{11} = \frac{C^{(1)}_{22} + C^{(2)}_{22}}{\left[C^{(1)}_{11} + 2C^{(2)}_{11}\right]\left[C^{(1)}_{22} + C^{(2)}_{22}\right] - C^{(1)}_{12}C^{(1)}_{21}}, \tag{3}$$

$$D_{12} = -\frac{C^{(1)}_{12}/2}{\left[C^{(1)}_{11} + 2C^{(2)}_{11}\right]\left[C^{(1)}_{22} + C^{(2)}_{22}\right] - C^{(1)}_{12}C^{(1)}_{21}}. \tag{4}$$

The components of the elastic tensors $C^{(1)}_{ij}$ and $C^{(2)}_{ij}$ have been defined in Eqs. (67) and (68) of Ju and Sun (2000).

For the uniaxial loading, the effective yield function given by Eq. (81) in Ju and Sun (2000) becomes

$$\bar{F}(\bar{\sigma}_{11}, \bar{e}^{\mathrm{p}}) = (1-\phi)\sqrt{\bar{T}^{(1)}_{11} + 2\bar{T}^{(2)}_{11}}\ \bar{\sigma}_{11} - \sqrt{\tfrac{2}{3}}[\sigma_{\mathrm{y}} + h(\bar{e}^{\mathrm{p}})^q], \tag{5}$$

where ϕ denotes the volume fraction of particles, σ_{y} signifies the initial yield stress, h and q designate the linear and exponential isotropic hardening parameters, respectively, and $\bar{e}^{\mathrm{p}}$ defines the effective equivalent plastic strain. In addition, the second-rank tensors $\bar{\mathbf{T}}^{(1)}$ and $\bar{\mathbf{T}}^{(2)}$ have been defined in Eqs. (61) and (62) in Part I of this sequel. Moreover, the overall incremental plastic strain defined by Eq. (84) in Ju and Sun (2000) reduces to

$$[\Delta\bar{\epsilon}_{ij}^{\mathrm{p}}] = \frac{(1-\phi)\ \Delta\lambda}{\sqrt{\bar{T}_{11}^{(1)} + 2\bar{T}_{11}^{(2)}}} \begin{bmatrix} \bar{T}_{11}^{(1)} + 2\bar{T}_{11}^{(2)} & 0 & 0 \\ 0 & \bar{T}_{12}^{(1)} & 0 \\ 0 & 0 & \bar{T}_{12}^{(1)} \end{bmatrix}, \tag{6}$$

where $\Delta\lambda$ is the incremental plastic consistency parameter.

For the special case of the monotonically increasing uniaxial loading condition, the overall strain–stress relationship can be derived by integrating Eqs. (2) and (6) as follows:

$$[\bar{\epsilon}_{ij}] = \begin{bmatrix} D_{11} & 0 & 0 \\ 0 & D_{12} & 0 \\ 0 & 0 & D_{12} \end{bmatrix} \bar{\sigma}_{11} + \frac{(1-\phi)\lambda}{\sqrt{\bar{T}_{11}^{(1)} + 2\bar{T}_{11}^{(2)}}} \begin{bmatrix} \bar{T}_{11}^{(1)} + 2\bar{T}_{11}^{(2)} & 0 & 0 \\ 0 & \bar{T}_{12}^{(1)} & 0 \\ 0 & 0 & \bar{T}_{12}^{(1)} \end{bmatrix}, \tag{7}$$

where the positive plastic consistency parameter $\lambda = \sum \Delta\lambda$ is solved from the nonlinear equation obtained by enforcing the plastic consistency condition $\bar{F} = 0$. Accordingly, λ can be determined as

$$\lambda = \frac{1}{\sqrt{2/3}(1-\phi)} \left[\frac{(1-\phi)\sqrt{3[\bar{T}_{11}^{(1)} + 2\bar{T}_{11}^{(2)}]/2}\ \bar{\sigma}_{11} - \sigma_{\mathrm{y}}}{h} \right]^{1/q}. \tag{8}$$

Therefore, from Eq. (7), the overall stress–strain curves for PRMMCs can be computed in terms of the volume fraction, aspect ratio, elastic properties of the reinforcements, as well as elastic and plastic parameters of the matrix material.

2.2. Numerical simulations and experimental comparisons

In this article, unless noted otherwise, the matrix material is taken as an aluminum alloy with Young's modulus $E_{\mathrm{m}} = 70$ GPa, Poisson's ratio $\nu_{\mathrm{m}} = 0.3$, the initial uniaxial yield stress $\sigma_{\mathrm{y}} = 300$ MPa, and the linear and exponential isotropic hardening parameters $h = 1000$ MPa and $q = 0.5$. Furthermore, we employ Young's modulus $E_{\mathrm{p}} = 450$ GPa and Poisson's ratio $\nu_{\mathrm{p}} = 0.2$ for the reinforcements (similar to the elastic properties of the SiC particles).

To illustrate the overall elastoplastic stress–strain behavior of PRMMCs under uniaxial tension, we first perform simulations in Fig. 1(a)–(d). In particular, Fig. 1(a) shows that Young's modulus, the initial yield strength and the plastic hardening modulus increase as the volume fraction of particles increases. This demonstrates the strengthening effect of PRMMCs. It is recalled from Part I of this sequel that the near-field direct particle interactions are not included, although the far-field interactions are accounted for. Therefore, we should avoid high particle volume fractions. Fig. 1(b) displays the effect of reinforcement shape on the mechanical behavior of PRMMCs with the same volume fraction of particles. The elasto-plastic behavior of PRMMCs is dependent on the aspect ratio α of spheroidal particles, especially during the plastic range. According to Fig. 1(b), PRMMCs reinforced with prolate spheroidal particles ($\alpha > 1$) are the most effective for the strengthening effect of composites. The above observation is in good agreement with, for example, Bao et al. (1991), Lee and Mear (1991), Li (1992), Li and Ponte Castaneda (1994), and Qiu and Weng (1995). The strengthening effect of PRMMCs containing aligned *oblate* spheroidal particles is not significant when compared to that of prolate particles. Again, from Part I, it is noted that extreme values for the aspect ratio should be avoided.

It is of interest to consider the elastoplastic behavior of PRMMCs with different contrast ratios in Young's modulus between the constituents. Fig. 1(c) indicates that higher Young's modulus of particles leads to higher elastic and plastic stress–strain responses and therefore more pronounced strengthening effect. Since the particles are always assumed to be elastic, stiffer stress–strain response over the matrix

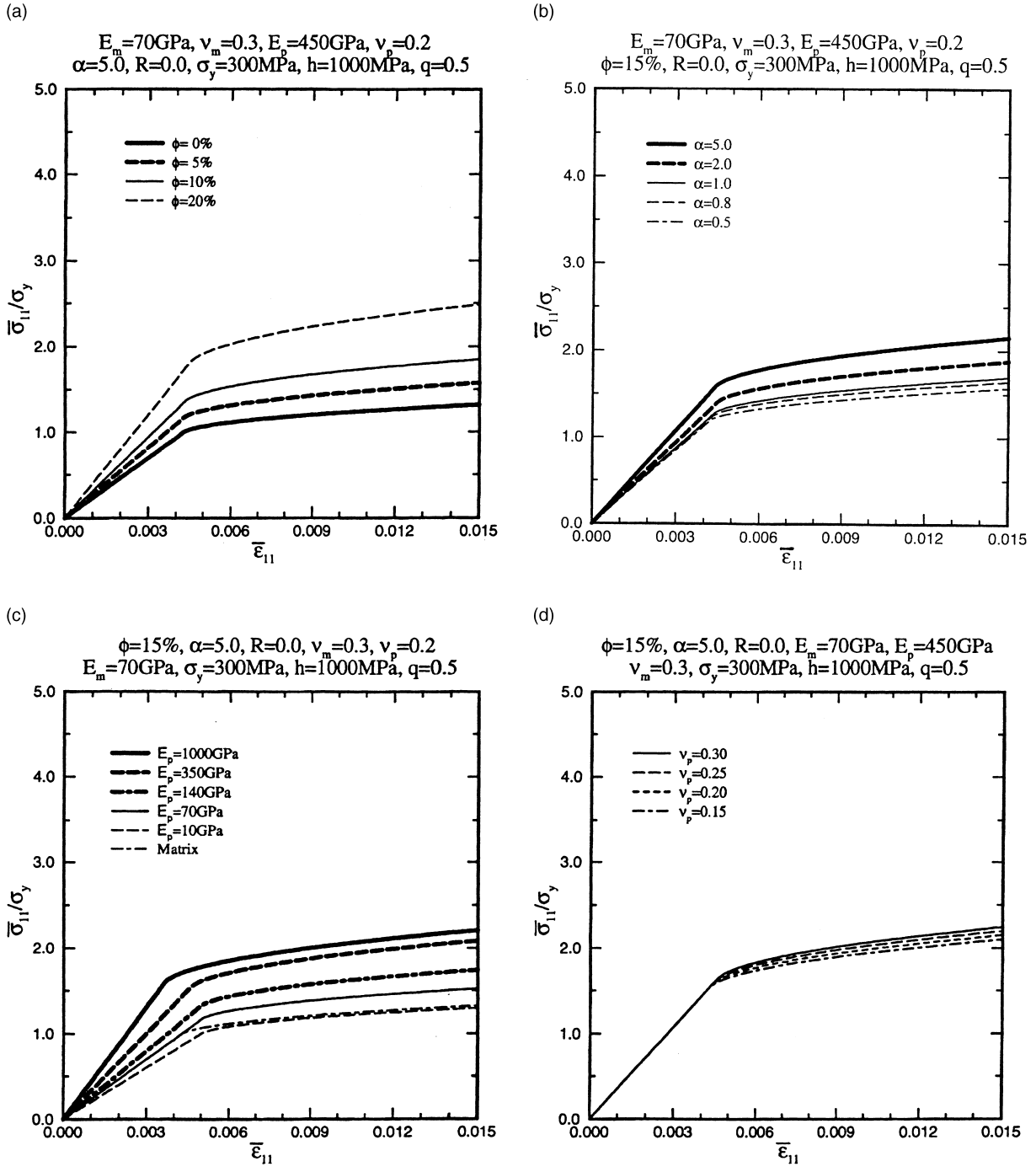

Fig. 1. Effects of (a) volume fractions, (b) aspect ratios, (c) Young's moduli, and (d) Poisson's ratios of particles on the normalized uniaxial elastoplastic behavior of PRMMCs.

response is observed. Even when Young's modulus of particles is the same as that of the matrix, the overall yield strength and plastic work hardening rate are higher than those of the matrix material. However, if Young's modulus of the particles is much lower than that of the matrix (e.g., $E_p = 10$ GPa and $E_m = 70$ GPa), the composite behavior will eventually fall below the stress–strain curve of the matrix-only material. In contrast, as seen from Fig. 1(d), there are no significant differences in the stress–strain behavior when Poisson's ratio of the particles varies.

Furthermore, in order to demonstrate the capability of the proposed formulation, we compare our predictions with the experimental data reported by Christman et al. (1989a,b). In their experiments, uniaxial stress–strain curves were recorded for the 2124 aluminum alloy reinforced with 13.2% SiC whiskers (SiC_w). It is noted that most whiskers become aligned right after the extrusion process during the fabrication of PRMMCs. The aspect ratio of whiskers reported in their experiments is about 5. In general, the shape of a whisker is more like a cylinder than a spheroid. Here, we follow the method proposed by Li and Ponte Castaneda (1994) to simulate whiskers by spheroids. The volume of a whisker is the same as that of an "equivalent" prolate spheroid such that the volume fraction of reinforcements remains the same for the actual composite and the "equivalent" composite. The radius of the cross-section of a whisker is assumed to be equal to the shorter semi-axis of a prolate spheroid. As a result, the aspect ratio of an "equivalent" spheroid is one and a half times of that of a whisker. Based on the general material descriptions documented in Christman et al. (1989a,b), Tvergaard (1990) and Hom (1992), the elastoplastic properties of the matrix and the elastic properties of the SiC whiskers, respectively, are selected as $E_m = 60$ GPa, $\nu_m = 0.3$, $\sigma_y = 290$ MPa, $h = 700$ MPa, $q = 0.55$, and $E_p = 450$ GPa, $\nu_p = 0.2$.

Fig. 2 exhibits the comparisons among our theoretical predictions, the experimental data by Christman et al. (1989a,b), and the finite element periodic unit-cell models (the overlapping and side-by-side cases) by Hom (1992) for SiC_w/Al composites. It is observed that the present predictions compare well with the experimental data in the elastic range and in the latter part of the plastic range. The more noticeable

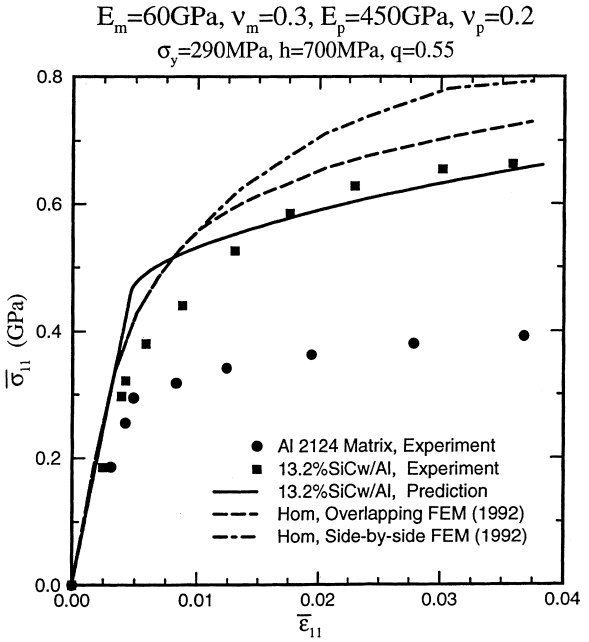

Fig. 2. Comparisons of uniaxial stress–strain responses with experimental data (Christman et al., 1989a,b) and FEM periodic unit-cell models (Hom, 1992) for SiC_w/Al composites.

deviation between the predictions and experimental data is in the initial part of the plastic range. On the other hand, the three-dimensional finite element simulations of Hom (1992) overestimate the stress–strain behavior due to the constraints imposed by the periodic unit-cell models. The primary reason for the overestimation of the present predictions at the initial yielding stage is due to thermal residual stresses in PRMMCs produced by the mismatch of thermal expansion coefficients between the constituents during fabrication processes. In fact, as pointed out by several investigators such as Zahl and McMeeking (1991), Povirk et al. (1991), and Levy and Papazian (1991), residual stresses reduce the flow strengths of composites at the beginning stage of yielding. Additional reasons for the overestimated yield strength include the lower stress concentrations in the vicinity of the spheroidal particles than cylindrical whiskers with sharp edges, the effects of partial misalignment and local clustering of whiskers, and the effects of overestimated elastic stiffness of composites.

Papazian and Adler (1990) also investigated the mechanical behavior of either SiC particulate-reinforced or SiC whisker-reinforced 5456 aluminum alloy matrix composites. Fig. 3 shows the comparisons between the present model, the experimental data and finite element periodic unit-cell models by Levy and Papazian (1990). Following Papazian and Adler (1990) and Levy and Papazian (1990), the material properties are chosen as $E_m = 73$ GPa, $\nu_m = 0.33$, $\sigma_y = 230$ MPa, $h = 410$ MPa, $q = 0.4$, $E_p = 485$ GPa and $\nu_p = 0.2$. Moreover, the mean aspect ratio of whiskers is 4.1. Therefore, the equivalent aspect ratio of spheroids is taken as 1.5 times of that of whiskers for the reason discussed above. However, we employ the aspect ratio of 1 (not 1.5) to represent the aspect ratio of SiC particulates because the reinforcements are not like cylinders. It is seen from Fig. 3 that the agreement between our predictions and experimental data for particulate reinforced MMCs is much better than that for whisker reinforced MMCs. This is in part due to the fact that the present model becomes more accurate as the aspect ratio approaches one. We refer to Section 3 of Ju and Sun (2000) for relevant discussions. Another possible reason is that the effects of thermal residual stresses upon whisker composites are more significant than those upon particulate com-

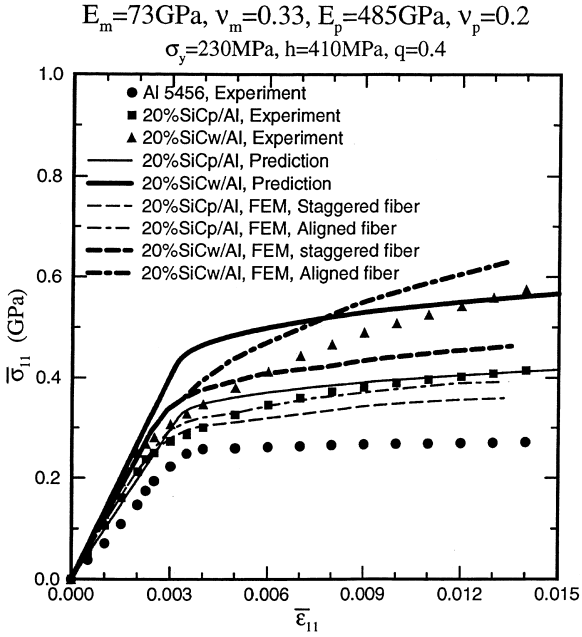

Fig. 3. Comparisons of uniaxial stress–strain responses with experimental data (Papazian and Adler, 1990) and FEM periodic unit-cell models (Levy and Papazian, 1990) for SiC_w/Al and SiCp/Al composites.

posites during the initial yielding stage. An additional reason is that misalignment does exist for whiskers but not for particulates. Furthermore, Christman et al. (1989b) indicated that effects of reinforcement clustering on the overall stress–strain behavior of MMCs are markedly less pronounced for unit aspect ratio than for whisker reinforcements. In addition, Fig. 3 exhibits the three-dimensional finite element results of Levy and Papazian (1990) for both particulate and whisker reinforced MMCs with either staggered or aligned array of periodic fibers. We observe that the difference between our theoretical closed-form predictions and finite element results for particulate reinforced MMCs is much less than that for whisker reinforced MMCs. The simplicity and compactness of the proposed method is noted.

3. Mechanical behavior of PRMMCs under purely hydrostatic tension

The von Mises J_2-theory is very popular in metal plasticity. A metal obeying the J_2-theory will never yield under the purely hydrostatic loading. However, the overall responses of PRMMCs under the purely hydrostatic loading should exhibit plastic yielding behavior; see e.g., Qiu and Weng (1992). In this section, we examine whether the present formulation is capable of predicting the elastoplastic behavior under the purely hydrostatic tension.

In this special case, the macroscopic stresses can be simplified as

$$\bar{\sigma}_{11} = \bar{\sigma}_{22} = \bar{\sigma}_{33} = \bar{\sigma}_{\mathrm{H}} > 0, \qquad \bar{\sigma}_{12} = \bar{\sigma}_{23} = \bar{\sigma}_{31} = 0, \tag{9}$$

where $\bar{\sigma}_{\mathrm{H}}$ denotes the hydrostatic tension. Following the assumption of isotropic hardening law, the effective yield criterion given in Eq. (81) by Ju and Sun (2000) can be written as

$$\bar{F}(\bar{\sigma}_{\mathrm{H}}, \bar{e}^{\mathrm{p}}) = (1-\phi)\Phi\bar{\sigma}_{\mathrm{H}} - \sqrt{\tfrac{2}{3}}[\sigma_{\mathrm{y}} + h(\bar{e}^{\mathrm{p}})^q], \tag{10}$$

where

$$\Phi = \sqrt{\bar{T}_{11}^{(1)} + 4\bar{T}_{12}^{(1)} + 4\bar{T}_{22}^{(1)} + 2\bar{T}_{11}^{(2)} + 4\bar{T}_{22}^{(2)}}. \tag{11}$$

Let us first investigate the initial yield strength $\bar{\boldsymbol{\sigma}}_{\mathrm{Hy}}$ of PRMMCs subject to the purely hydrostatic tension. By setting $h = 0$ and $q = 0$ in Eq. (10), the initial yield stress can be easily derived as

$$\frac{\bar{\sigma}_{\mathrm{Hy}}}{\sigma_{\mathrm{y}}} = \frac{\sqrt{2/3}}{(1-\phi)\Phi}. \tag{12}$$

From the expression of Φ, it can be shown that Φ goes to zero when the volume fraction of particles, ϕ, vanishes. This implies that the matrix material will never yield under hydrostatic loading. Therefore, the present formulation does recover the traditional J_2-plasticity theory when $\phi = 0$.

The normalized yield stresses $\bar{\sigma}_{\mathrm{Hy}}/\sigma_{\mathrm{y}}$ are plotted in Fig. 4(a)–(d) for different volume fractions of particles, aspect ratios of particles and phase contrast ratios $E_{\mathrm{p}}/E_{\mathrm{m}}$. It is clear that, with increasing volume fractions of particles in Fig. 4(a), the PRMMCs become easier to yield regardless of the aspect ratios of spheroidal particles. From Fig. 4(b), we observe that the yield stresses of PRMMCs under purely hydrostatic loading are not sensitive to the aspect ratios of oblate particles. It seems that, from Fig. 4(c), at a lower volume fraction of particles (e.g., 5%), the maximum $\bar{\sigma}_{\mathrm{Hy}}$ occurs when α is near 1.6 (prolate). However, at a higher volume fraction (e.g., 20%), the $\bar{\sigma}_{\mathrm{Hy}}$ values monotonically decrease when the aspect ratios of prolate particles increase. In addition, Fig. 4(d) indicates that PRMMCs cannot yield when the elastic properties of the two constituents are identical. The overall yield stresses decrease rapidly for any particle volume fractions when the contrast ratio $E_{\mathrm{p}}/E_{\mathrm{m}}$ is not equal to 1.

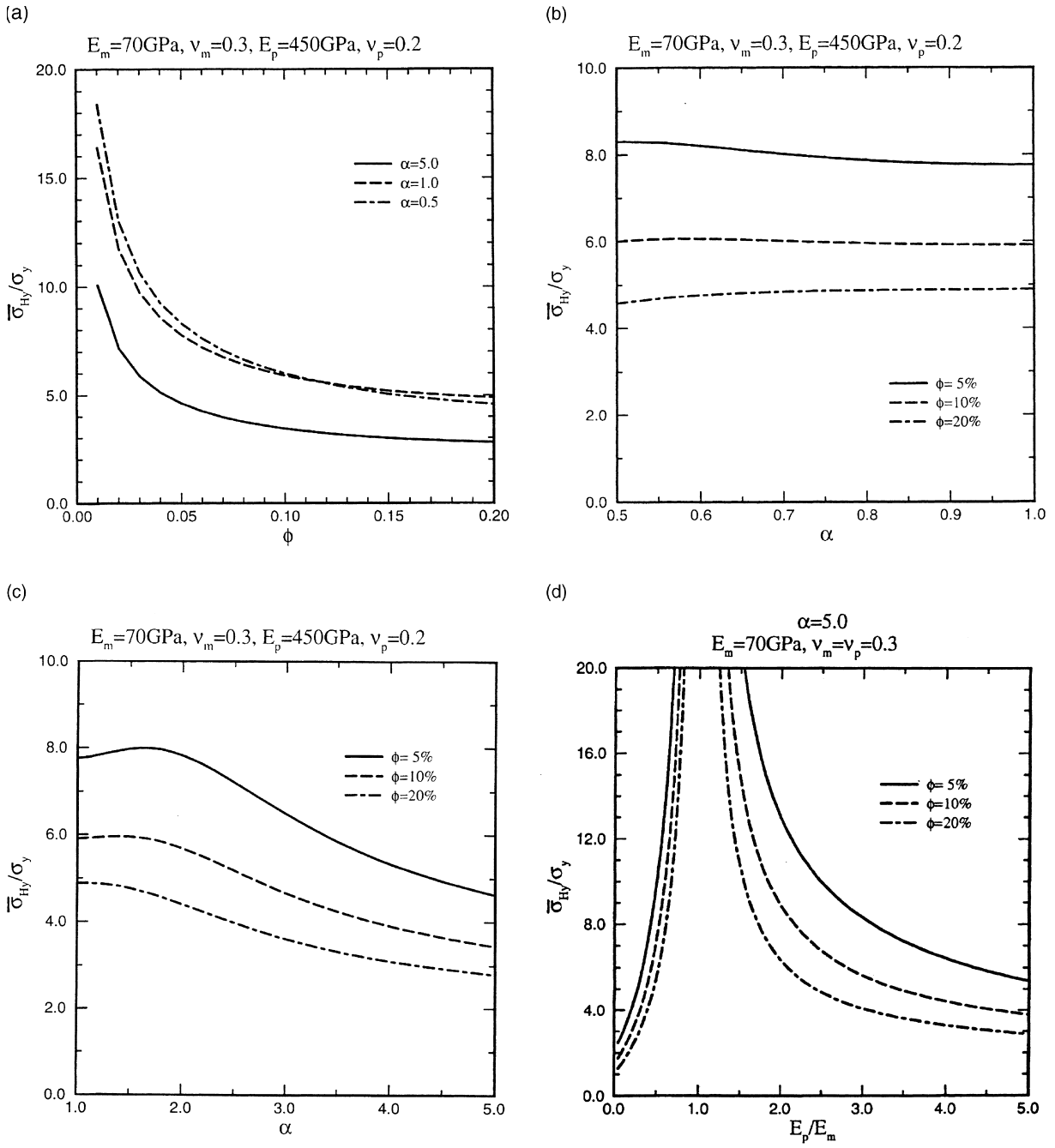

Fig. 4. Effects of (a) volume fractions, (b) oblate aspect ratios, (c) prolate aspect ratios, and (d) Young's moduli of particles on the normalized initial yield stresses of PRMMCs under pure hydrostatic loading.

After PRMMCs reach plastic yielding, the overall incremental plastic strains take the form:

$$[\Delta\bar{\epsilon}^{\mathrm{p}}_{ij}] = \frac{(1-\phi)\ \Delta\lambda}{\Phi}\begin{bmatrix} L_{11} & 0 & 0 \\ 0 & L_{22} & 0 \\ 0 & 0 & L_{22} \end{bmatrix}, \tag{13}$$

where

$$L_{11} = \bar{T}^{(1)}_{11} + 2\bar{T}^{(1)}_{12} + 2\bar{T}^{(2)}_{11}, \tag{14}$$

$$L_{22} = \bar{T}^{(1)}_{12} + 2\bar{T}^{(1)}_{22} + 2\bar{T}^{(2)}_{22}. \tag{15}$$

Eq. (13) is valid for any arbitrary loading and unloading step. Furthermore, under the monotonically increasing loading condition, the overall stress–strain relationship can be expressed as

$$[\bar{\epsilon}_{ij}] = \begin{bmatrix} D_{11}+2D_{12} & 0 & 0 \\ 0 & D_{12}+D_{22} & 0 \\ 0 & 0 & D_{12}+D_{22} \end{bmatrix}\bar{\sigma}_{\mathrm{H}} + \frac{(1-\phi)\lambda}{\Phi}\begin{bmatrix} L_{11} & 0 & 0 \\ 0 & L_{22} & 0 \\ 0 & 0 & L_{22} \end{bmatrix}, \tag{16}$$

where the first term of the right-hand side in the above equation represents the elastic strains, the second term is attributed to the plastic strains, and we have $\lambda = \sum \Delta\lambda$. In addition, D_{11} and D_{12} are defined in Eqs. (3) and (4), and

$$D_{22} = \frac{\left[C^{(1)}_{11} + 2C^{(2)}_{11}\right]/2}{\left[C^{(1)}_{11} + 2C^{(2)}_{11}\right]\left[C^{(1)}_{22} + C^{(2)}_{22}\right] - C^{(1)}_{12}C^{(1)}_{21}}. \tag{17}$$

The plastic consistency parameter can be computed as

$$\lambda = \frac{1}{\sqrt{2/3}(1-\phi)}\left[\frac{\sqrt{3/2}(1-\phi)\Phi\bar{\sigma}_{\mathrm{H}} - \sigma_{\mathrm{y}}}{h}\right]^{1/q}. \tag{18}$$

From Eq. (16), the plastic volumetric strain $\bar{\epsilon}^{\mathrm{p}}_{kk}$ can be derived as

$$\bar{\epsilon}^{\mathrm{p}}_{kk} = (1-\phi)\lambda\Phi. \tag{19}$$

With the help of $\bar{T}^{(1)}_{ij}$ and $\bar{T}^{(2)}_{ij}$ in Eqs. (42) and (43) of Part I of this sequel, the plastic volumetric strain is indeed nonzero unless the volume fraction of particles reduces to zero in the case of the matrix-only material with J_2-plasticity theory. Therefore, even though the matrix material is plastically incompressible, the composite as a whole is plastically compressible.

According to Eq. (16), the overall stress–strain curves of PRMMCs can be predicted for various volume fractions, aspect ratios and Young's moduli of particles. Under the purely hydrostatic tension, Fig. 5(a) shows that $\bar{\epsilon}_{11}$ strains along the aligned axisymmetric axis of prolate spheroids increase during the elastic phase. Subsequently, after yielding, $\bar{\epsilon}_{11}$ strains gradually decrease and eventually become negative (compressive). The reason for this behavior is that the plastic strains $\bar{\epsilon}^{\mathrm{p}}_{11}$ become negative once plastic yielding occurs due to the fact that the magnitude of combined negative lateral plastic strains from the 22- and 33-direction are greater than that from the 11-direction. However, the normalized stress–strain curves of $\bar{\sigma}_{22}$ vs. $\bar{\epsilon}_{22}$ in Fig. 5(b) and $\bar{\sigma}_{\mathrm{H}}$ vs. $\bar{\epsilon}_{kk}$ in Fig. 5(c) display monotonic behavior without "bend-over". Here, $\bar{\epsilon}_{kk}$ denotes the overall volumetric strain. In addition, PRMMCs with higher concentrations of particles are stiffer during the elastic range. By contrast, after yielding, PRMMCs with lower volume fractions of particles gradually become more effective in strengthening the stress–strain behavior under purely hydrostatic loading.

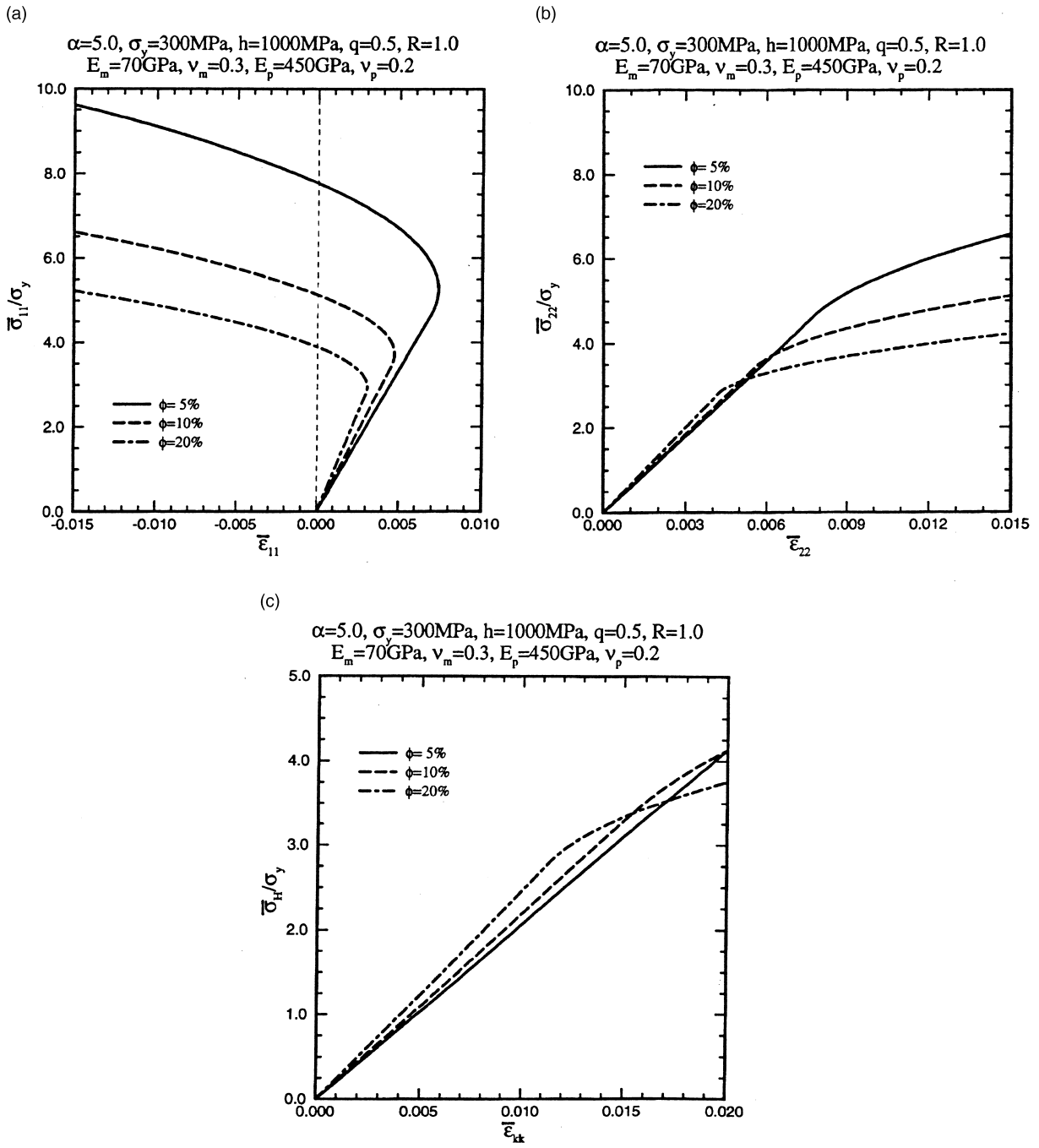

Fig. 5. Effects of volume fractions of particles on the normalized overall elastoplastic responses in the (a) 11-direction, (b) 22-direction, and (c) volumetric component for PRMMCs under pure hydrostatic loading.

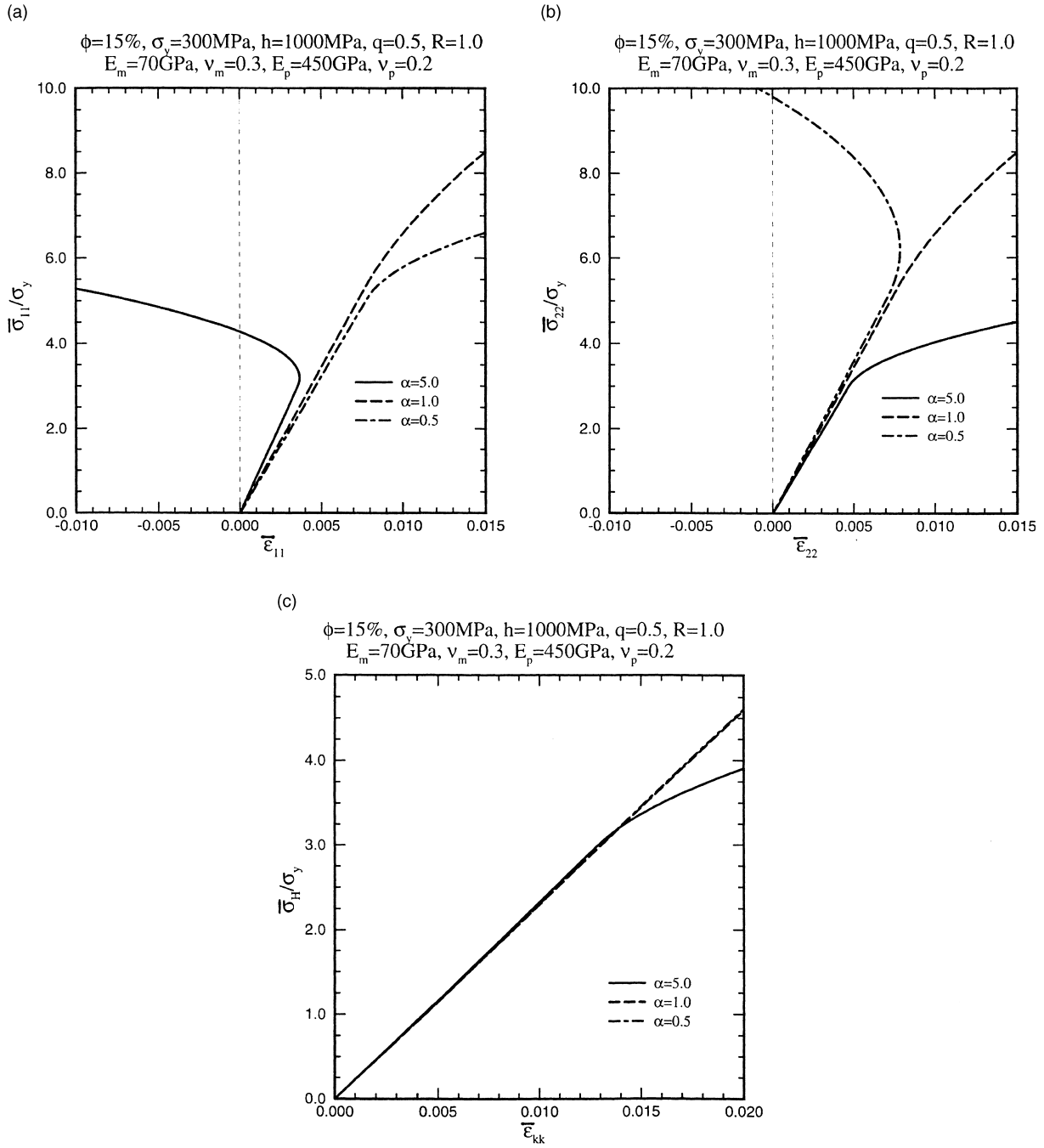

Fig. 6. Effects of aspect ratios of particles on the normalized overall elastoplastic responses in the (a) 11-direction, (b) 22-direction, and (c) volumetric component for PRMMCs under pure hydrostatic loading.

Fig. 6(a)–(c) exhibits the effects of aspect ratios of particles on the normalized overall stress–strain curves under the purely hydrostatic loading for the 11-direction, 22-direction and volumetric component, respectively. In particular, after yielding, Fig. 6(a)–(b) displays that $\bar{\epsilon}_{11}$ strain and $\bar{\epsilon}_{22}$ strain gradually decrease and eventually become negative along the *longer* axes of the prolate (Fig. 6(a), $\alpha = 5$) and oblate (Fig. 6(b), $\alpha = 0.5$) spheroids, respectively. The "bend-over" phenomenon does not occur for PRMMCs with spherical particles. Moreover, Fig. 6(c) again shows that the volumetric responses never go negative.

The influences of contrast ratios of Young's moduli on the elastoplastic behavior of PRMMCs under hydrostatic loading is illustrated in Fig. 7(a)–(c). We clearly observe that PRMMCs with the same elastic properties between the two constituents never yield. The "bend-over" phenomenon is noted in Fig. 7(a) along the aligned axisymmetric axis (11-direction) of prolate spheroids when Young's moduli of particles are stiffer than that of the matrix. On the other hand, no such phenomenon occurs when prolate spheroids feature weaker Young's modulus than that of the matrix, or when the stress–strain responses along the 22-direction are plotted (Fig. 7(b)).

It is concluded that the "bend-over" phenomenon takes place due to the spheroidal particle shape; i.e., $\alpha \neq 1$.

4. Mechanical behavior of PRMMCs under axisymmetric tension

In axisymmetric tension, the axisymmetric axis is parallel to the x_1-axis and the overall stresses read

$$\bar{\sigma}_{11} > 0, \qquad \bar{\sigma}_{22} = \bar{\sigma}_{33} = R\bar{\sigma}_{11}, \qquad \bar{\sigma}_{12} = \bar{\sigma}_{23} = \bar{\sigma}_{31} = 0, \tag{20}$$

where the stress ratio R is a real number and a function of loading history. Specifically, if $R = 0$, the uniaxial loading case will be recovered. On the other hand, $R = 1$ recovers the purely hydrostatic loading case.

For simplicity, only constant R is considered in this section. Therefore, from axisymmetric loading condition, the overall elastic strains are simplified as

$$[\bar{\epsilon}^{\mathrm{e}}_{ij}] = \begin{bmatrix} D_{11} + 2RD_{12} & 0 & 0 \\ 0 & D_{12} + RD_{22} & 0 \\ 0 & 0 & D_{12} + RD_{22} \end{bmatrix} \bar{\sigma}_{11}. \tag{21}$$

Furthermore, the yield criterion can be written as

$$\bar{F}(\bar{\sigma}_{11}, \bar{e}^{\mathrm{p}}) = (1-\phi)\Phi(R)\bar{\sigma}_{11} - \sqrt{\tfrac{2}{3}}[\sigma_{\mathrm{y}} + h(\bar{e}^{\mathrm{p}})^q] \leqslant 0, \tag{22}$$

where

$$\Phi(R) = \sqrt{\bar{T}^{(1)}_{11} + 2\bar{T}^{(2)}_{11} + 4R\bar{T}^{(1)}_{12} + 4R^2\left[\bar{T}^{(1)}_{22} + \bar{T}^{(2)}_{22}\right]}. \tag{23}$$

After the plastic yielding, the overall incremental plastic strains read

$$[\Delta\bar{\epsilon}^{\mathrm{p}}_{ij}] = \frac{(1-\phi)\,\Delta\lambda}{\Phi(R)} \begin{bmatrix} L_{11}(R) & 0 & 0 \\ 0 & L_{22}(R) & 0 \\ 0 & 0 & L_{22}(R) \end{bmatrix} \tag{24}$$

in which

$$L_{11}(R) = \bar{T}^{(1)}_{11} + 2R\bar{T}^{(1)}_{12} + 2\bar{T}^{(2)}_{11}, \tag{25}$$

$$L_{22}(R) = \bar{T}^{(1)}_{12} + 2R\bar{T}^{(1)}_{22} + 2R\bar{T}^{(2)}_{22}. \tag{26}$$

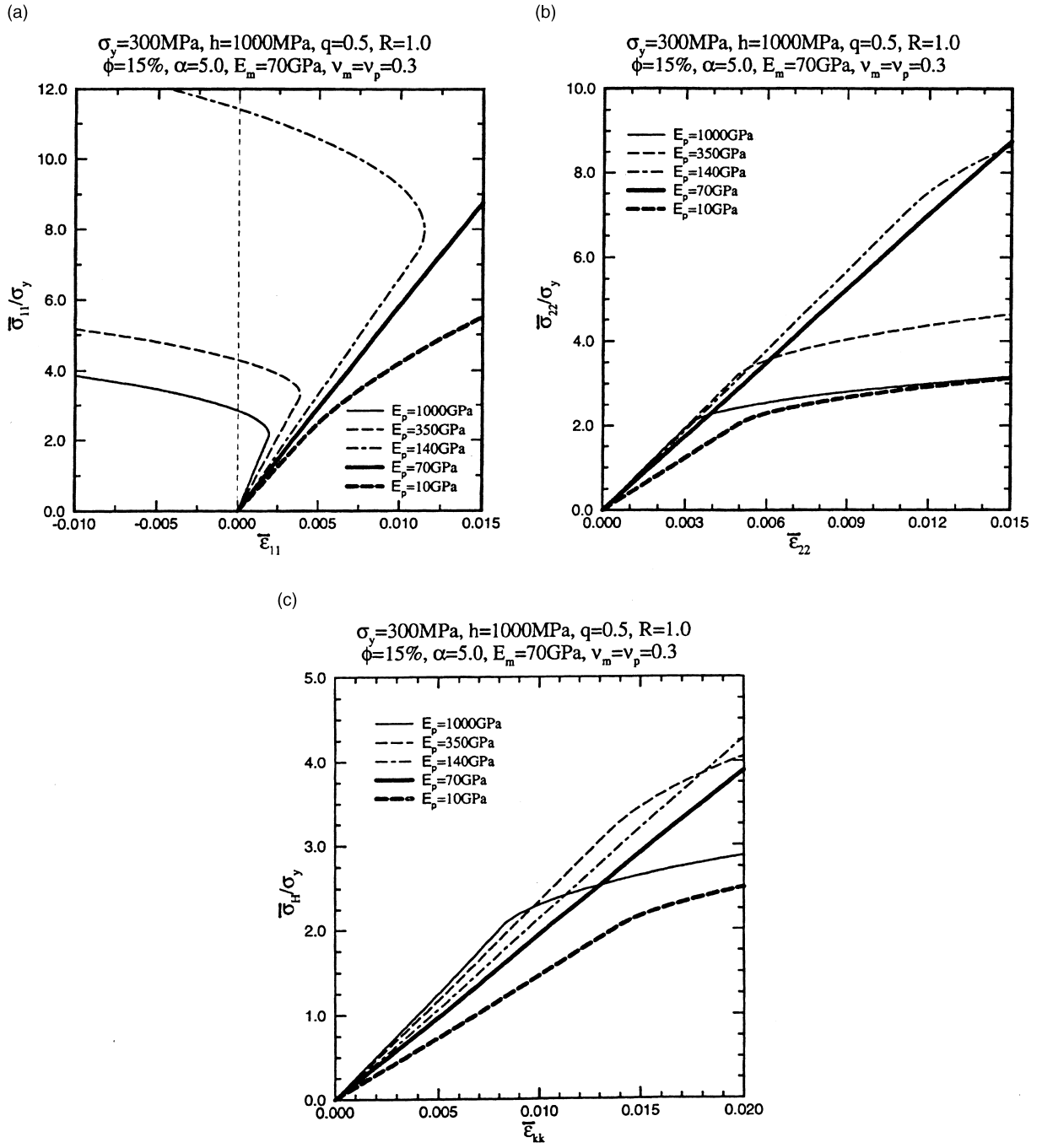

Fig. 7. Effects of Young's moduli of particles on the normalized overall elastoplastic responses in the (a) 11-direction, (b) 22-direction, and (c) volumetric component for PRMMCs under pure hydrostatic loading.

Again, Eq. (24) is valid for any arbitrary loading and unloading step. As before, if the loading is monotonically increasing, then $\Delta\bar{\epsilon}^{\mathrm{p}}_{ij}$ and $\Delta\lambda$ in Eq. (24) can be replaced by $\bar{\epsilon}^{\mathrm{p}}_{ij}$ and λ, respectively, to render the overall (cumulative) plastic strains. The plastic consistency parameter λ can be determined as

$$\lambda = \frac{1}{\sqrt{2/3}(1-\phi)}\left[\frac{\sqrt{3/2}(1-\phi)\Phi(R)\bar{\sigma}_{11} - \sigma_{\mathrm{y}}}{h}\right]^{1/q}. \tag{27}$$

Therefore, by specifying the overall stress $\bar{\sigma}_{11}$ and the stress ratio R, the overall strains $\bar{\epsilon}_{11}$ and $\bar{\epsilon}_{22}$ can be computed with the combination of Eqs. (21) and (24).

Effects of R on mechanical behavior of PRMMCs are shown in Fig. 8(a)–(d). It is noted that the stress ratio R has a significant impact on the overall responses of PRMMCs. In Fig. 8(a) and (c), when R increases from zero, the stress–strain behavior $\bar{\sigma}_{11}$ vs. $\bar{\epsilon}_{11}$ of the axisymmetric direction of either prolate or oblate spheroids becomes less nonlinear until the previously mentioned "bend-over" phenomenon occurs. By contrast, as R decreases from 1.5, the corresponding behavior $\bar{\sigma}_{22}$ vs. $\bar{\epsilon}_{22}$ of the lateral direction acts less nonlinearly until the "bend-over" again takes place as shown in Fig. 8(b) and (d).

5. Initial yield surfaces of PRMMCs

Under general loading condition, the initial yield surface of PRMMCs can be obtained from Eq. (81) of Ju and Sun (2000) as

$$\bar{\boldsymbol{\sigma}} : \bar{\mathbf{T}} : \bar{\boldsymbol{\sigma}} = \frac{2\sigma_{\mathrm{y}}^2}{3(1-\phi)^2}, \tag{28}$$

where $\bar{\mathbf{T}}$ is a fourth-rank tensor defined by Eq. (60) of Ju and Sun (2000). Alternatively, we can express Eq. (28) in terms of the component form:

$$\left[\bar{T}^{(1)}_{11} + 2\bar{T}^{(2)}_{11}\right]\bar{\sigma}^2_{11} + \left[\bar{T}^{(1)}_{22} + 2\bar{T}^{(2)}_{22}\right]\left(\bar{\sigma}^2_{22} + \bar{\sigma}^2_{33}\right) + 4\bar{T}^{(2)}_{12}\left(\bar{\sigma}^2_{12} + \bar{\sigma}^2_{13}\right) + 4\bar{T}^{(2)}_{22}\bar{\sigma}^2_{23} + 2\bar{T}^{(1)}_{12}\bar{\sigma}_{11}(\bar{\sigma}_{22} + \bar{\sigma}_{33}) + 2\bar{T}^{(1)}_{22}\bar{\sigma}_{22}\bar{\sigma}_{33} = \frac{2\sigma_{\mathrm{y}}^2}{3(1-\phi)^2}. \tag{29}$$

As demonstrated by Drucker (1951, 1959), a necessary restriction for a valid yield surface is convexity. Recently, Voyiadjis and Thiagarajan (1995) proposed a phenomenological anisotropic yield surface for unidirectionally reinforced MMCs and proved the convexity of their yield surface. We shall prove the convexity of our proposed yield surface in the following.

In order to achieve this objective, it is more convenient to employ the vector form of the second-rank stress tensor $\bar{\boldsymbol{\sigma}}_{ij}$, which is defined as

$$\{\bar{\sigma}_i\} = \{\bar{\sigma}_{11}, \bar{\sigma}_{22}, \bar{\sigma}_{33}, \bar{\sigma}_{23}, \bar{\sigma}_{31}, \bar{\sigma}_{12}\}^{\mathrm{T}}. \tag{30}$$

Accordingly, the yield surface in Eq. (28) can be rewritten as

$$\{\bar{\sigma}_i\}^{\mathrm{T}}[\bar{T}_{ij}]\{\bar{\sigma}_j\} = \frac{2\sigma_{\mathrm{y}}^2}{3(1-\phi)^2}, \tag{31}$$

where the matrix form of $\bar{T}_{ij}$ is defined as

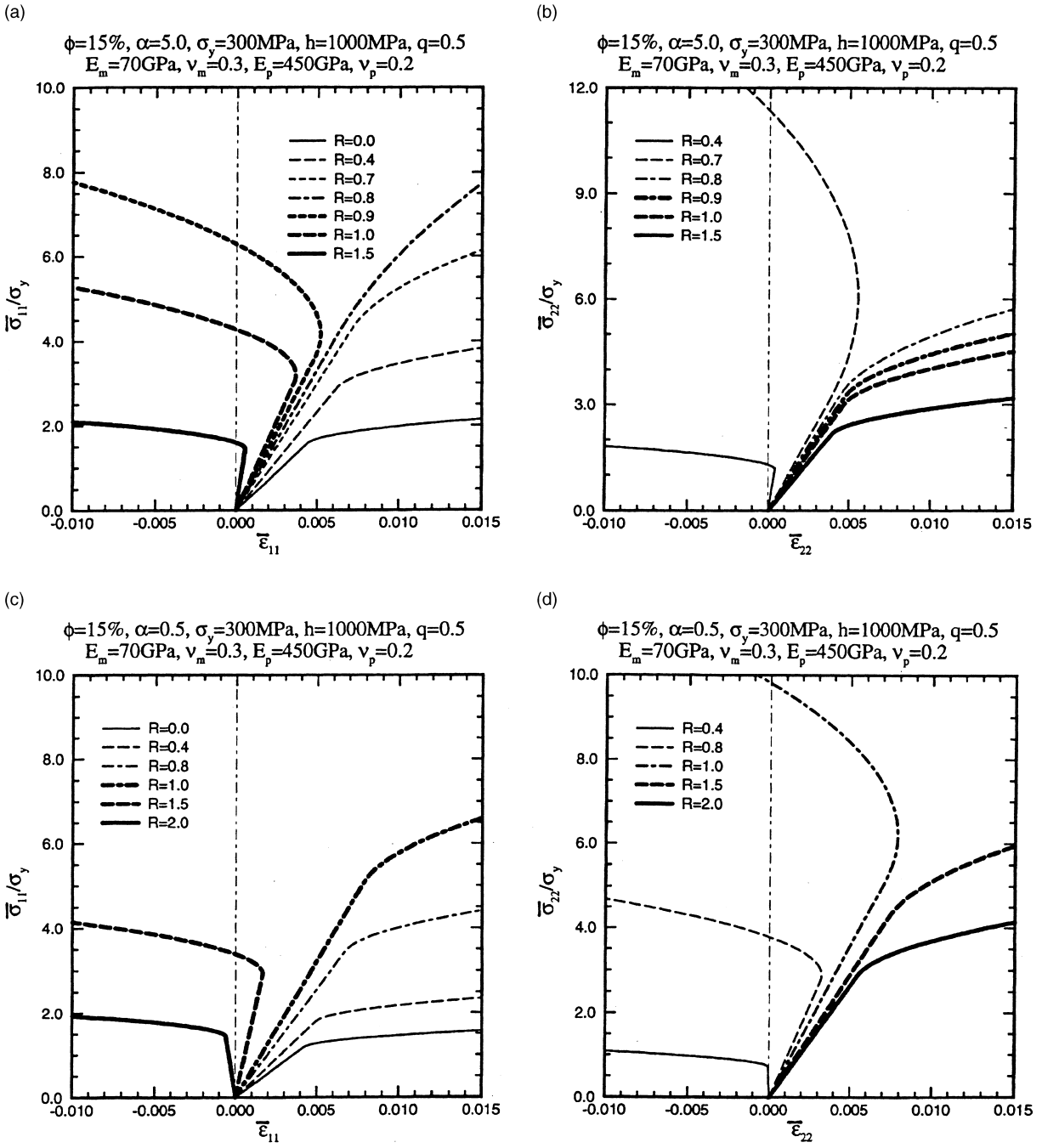

Fig. 8. Effects of stress ratios on the normalized overall elastoplastic responses in the (a) 11-direction (prolate spheroids with $\alpha = 5$), (b) 22-direction (prolate spheroids with $\alpha = 5$), (c) 11-direction (oblate spheroids with $\alpha = 0.5$), and (d) 22-direction (oblate spheroids with $\alpha = 0.5$) for PRMMCs under axisymmetric loading.

$$[\bar{T}_{ij}] = \begin{bmatrix} \bar{T}_{11}^{(1)} + 2\bar{T}_{11}^{(2)} & \bar{T}_{12}^{(1)} & \bar{T}_{12}^{(1)} & 0 & 0 & 0 \\ \bar{T}_{12}^{(1)} & \bar{T}_{22}^{(1)} + 2\bar{T}_{22}^{(2)} & \bar{T}_{22}^{(1)} & 0 & 0 & 0 \\ \bar{T}_{12}^{(1)} & \bar{T}_{22}^{(1)} & \bar{T}_{22}^{(1)} + 2\bar{T}_{22}^{(2)} & 0 & 0 & 0 \\ 0 & 0 & 0 & 4\bar{T}_{22}^{(2)} & 0 & 0 \\ 0 & 0 & 0 & 0 & 4\bar{T}_{12}^{(2)} & 0 \\ 0 & 0 & 0 & 0 & 0 & 4\bar{T}_{12}^{(2)} \end{bmatrix}. \tag{32}$$

All eigenvalues of the above matrix are investigated here so as to prove the convexity of the proposed yield surface. The convexity of the yield surface is guaranteed if all eigenvalues are positive, i.e., if the matrix $\bar{T}_{ij}$ is positive-definite.

The six eigenvalues $\beta_i (i = 1, 2, \ldots 6)$ of the matrix $[\bar{T}_{ij}]$ are solved as follows:

$$\beta_1 = 2\bar{T}_{22}^{(2)}, \tag{33}$$

$$\beta_2 = 4\bar{T}_{12}^{(2)}, \tag{34}$$

$$\beta_3 = 4\bar{T}_{12}^{(2)}, \tag{35}$$

$$\beta_4 = 4\bar{T}_{22}^{(2)}, \tag{36}$$

$$\beta_5 = \tfrac{1}{2}\bar{T}_{11}^{(1)} + \bar{T}_{22}^{(1)} + \bar{T}_{11}^{(2)} + \bar{T}_{22}^{(2)} - \tfrac{1}{2}\sqrt{\left[\bar{T}_{11}^{(1)} + 2\bar{T}_{11}^{(2)} - 2\bar{T}_{22}^{(1)} - 2\bar{T}_{22}^{(2)}\right]^2 + 8\left[\bar{T}_{12}^{(1)}\right]^2}, \tag{37}$$

$$\beta_6 = \tfrac{1}{2}\bar{T}_{11}^{(1)} + \bar{T}_{22}^{(1)} + \bar{T}_{11}^{(2)} + \bar{T}_{22}^{(2)} + \tfrac{1}{2}\sqrt{\left[\bar{T}_{11}^{(1)} + 2\bar{T}_{11}^{(2)} - 2\bar{T}_{22}^{(1)} - 2\bar{T}_{22}^{(2)}\right]^2 + 8\left[\bar{T}_{12}^{(1)}\right]^2}. \tag{38}$$

After extensive, lengthy yet straightforward calculations, it is found that all the eigenvalues are positive. Therefore, the proposed yield surface is convex.

We will now illustrate the initial yield surfaces of PRMMCs under the axisymmetric loading in which the axisymmetric axis is parallel to the x_1-axis. For convenience, the yield surfaces can be displayed in terms of the mean stress $\bar{\sigma}_m$ and the effective deviatoric stress $\bar{\sigma}_e$ which are defined as follows:

$$\bar{\sigma}_m = \tfrac{1}{3}\bar{\sigma}_{kk} = \frac{1}{3}(\bar{\sigma}_{11} + 2\bar{\sigma}_{22}), \tag{39}$$

$$\bar{\sigma}_e = \sqrt{\tfrac{3}{2}\bar{s}_{ij}\bar{s}_{ij}} = \bar{\sigma}_{11} - \bar{\sigma}_{22}, \tag{40}$$

where $\bar{s}_{ij}$ is the overall deviatoric stress tensor.

Figs. 9 and 10 exhibit the normalized overall yield surfaces of PRMMCs with either harder ($E_p > E_m$) or softer ($E_p < E_m$) particles under axisymmetric loading by using the mean stress $\bar{\sigma}_m$ and the effective deviatoric stress $\bar{\sigma}_e$. From Fig. 9(a)–(b), it is observed that the initial yield point in terms of $\bar{\sigma}_e$ or $\bar{\sigma}_m$ increases or decreases, respectively, with increasing ϕ for prolate spheroids. In particular, the decrease of yield point in the $\bar{\sigma}_m$ value has previously been discussed in Section 3 under pure hydrostatic tension. Near the small intersection region of all yield surfaces, the yield points are insensitive to different volume fractions of prolate spheroids. In addition, Fig. 10(a) shows that the yield point in $\bar{\sigma}_e$ increases with increasing aspect ratio α for PRMMCs with harder particles. By contrast, the yield point in $\bar{\sigma}_e$ is not very sensitive to the aspect ratio α for PRMMCs with softer particles in Fig. 10(b). Fig. 10(a) illustrates that the composite with harder spherical particles is more difficult to yield than that with harder oblate spheroids. On the other

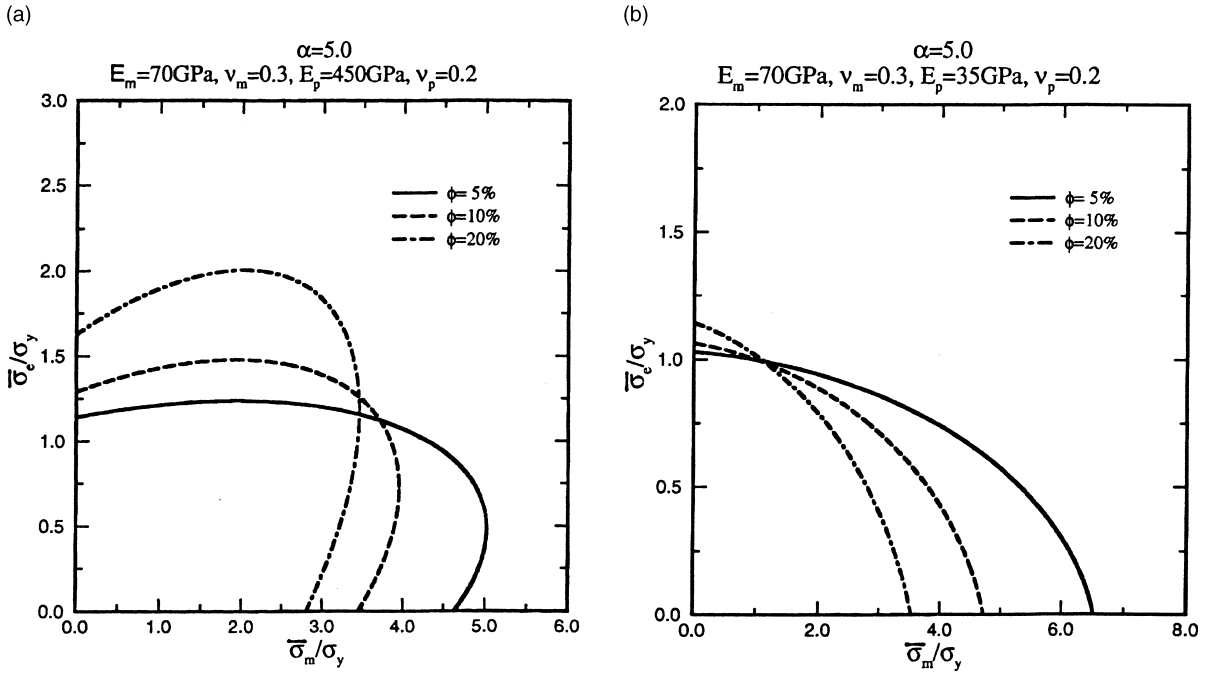

Fig. 9. Effects of volume fractions of prolate spheroidal (a) harder and (b) softer particles on the normalized overall initial yield surfaces of PRMMCs.

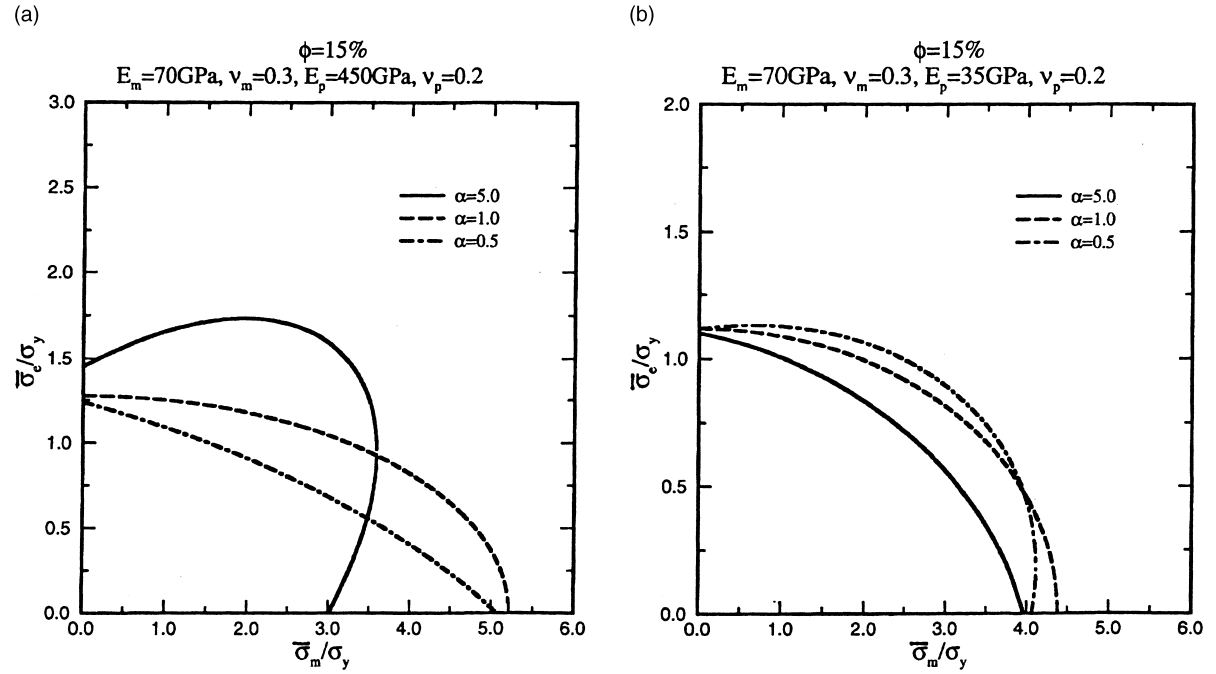

Fig. 10. Effects of aspect ratios of (a) harder and (b) softer particles on the normalized overall initial yield surfaces of PRMMCs.

hand, Fig. 10(b) demonstrates that the composite with softer prolate particles is easier to yield than that of softer spherical particles. Generally speaking, from Figs. 9 and 10, there is no clear choice of ϕ or α which would universally increase the yield surface under all loading conditions. This observation suggests that the selection of optimal ϕ or α for PRMMCs depends on the applied loading conditions.

There exist some experimental data on the yield surfaces of PRMMCs under multiaxial loading. For example, Zhu et al. (1995) performed the biaxial tension–torsion tests to investigate the yield surfaces of the silicon particle reinforced aluminum matrix composites. For this special case, the yield criterion in Eq. (29) for our proposed model takes the form

$$\left[\bar{T}_{11}^{(1)} + 2\bar{T}_{11}^{(2)}\right]\left(\frac{\bar{\sigma}_{11}}{\sigma_y}\right)^2 + 4\bar{T}_{12}^{(2)}\left(\frac{\bar{\tau}_\theta}{\sigma_y}\right)^2 = \frac{2}{3(1-\phi)^2}, \tag{41}$$

where the torsional shear stress $\bar{\tau}_\theta$ reads

$$\bar{\tau}_\theta = \sqrt{\bar{\sigma}_{12}^2 + \bar{\sigma}_{13}^2}. \tag{42}$$

Emanating from Zhu et al. (1995), the aspect ratio of harder particles is taken as $\alpha = 1$, and the volume fractions of particles are chosen as $\phi = 9.7\%$ and 19.5%. Furthermore, the material properties of the aluminum matrix are reported as $E_m = 70$ GPa, $\nu_m = 0.3$, and $\sigma_y = 68.5$ MPa (Zhu et al., 1995). The elastic constants of silicon particles are chosen as $E_p = 107$ GPa and $\nu_p = 0.2$ (Lynch et al., 1966) in the following experimental validation.

Fig. 11 renders the comparison between the present predictions and experimental data on the yield surfaces of particulate reinforced aluminum matrix composites for different particle volume fractions (Zhu

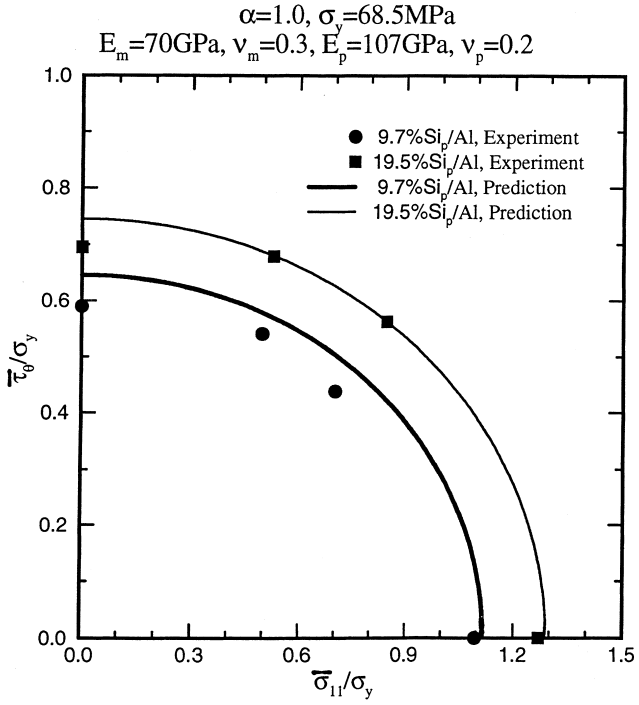

Fig. 11. Comparisons with experimental yield surfaces of Si/Al composites (Zhu et al., 1995).

et al., 1995). Solid lines correspond to the current predictions and the discrete points refer to the experimental data. Generally, the yield surfaces of Si/Al composites are well modeled by the present formulation, although some discrepancy in shear strength exists. It seems that the proposed yield criterion for PRMMCs is quite satisfactory.

Furthermore, to illustrate the capability of the proposed framework, we proceed to predict initial yield stresses for an elastically incompressible ductile matrix containing randomly located yet aligned spheroidal voids. This special problem is one of main topics in micromechanical damage mechanics and has attracted broad interest from many researchers. For example, Ponte Castaneda (1991) presented mathematical upper bounds for the yield surfaces of porous materials. Moreover, Qiu and Weng (1993, 1995) derived a yield criterion for ductile matrix materials containing aligned spheroidal inclusions through an energy approach. They prove that their results are identical to Ponte Castaneda's bounds if the matrix material is elastically incompressible and the inclusions are voids. In such a situation, as discussed in detail by Ju and Tseng (1996) and Ju and Lee (2000), the present initial yield criterion under axisymmetric loading in Eq. (28) is recast as

$$\left[\bar{T}_{11}^{(1)} + 2\bar{T}_{11}^{(2)}\right]\left[\frac{\bar{\sigma}_{11}}{\sigma_y}\right]^2 + 4\bar{T}_{12}^{(1)}\frac{\bar{\sigma}_{11}}{\sigma_y}\frac{\bar{\sigma}_{22}}{\sigma_y} + 4\left[\bar{T}_{22}^{(1)} + \bar{T}_{22}^{(2)}\right]\left[\frac{\bar{\sigma}_{22}}{\sigma_y}\right]^2 = \frac{2}{3}. \tag{43}$$

The above equation can also be expressed in terms of the mean stress $\bar{\sigma}_m$ and the effective deviatoric stress $\bar{\sigma}_e$.

The comparisons between the present initial yield surfaces and the mathematical upper bounds under axisymmetric loading with different volume fractions and aspect ratios of voids are plotted in Fig. 12(a)–(b), in which solid lines correspond to the upper bounds and the dash lines refer to the present predictions. It is observed from Fig. 12(a) that our predictions fall within the corresponding upper bounds. In addition,

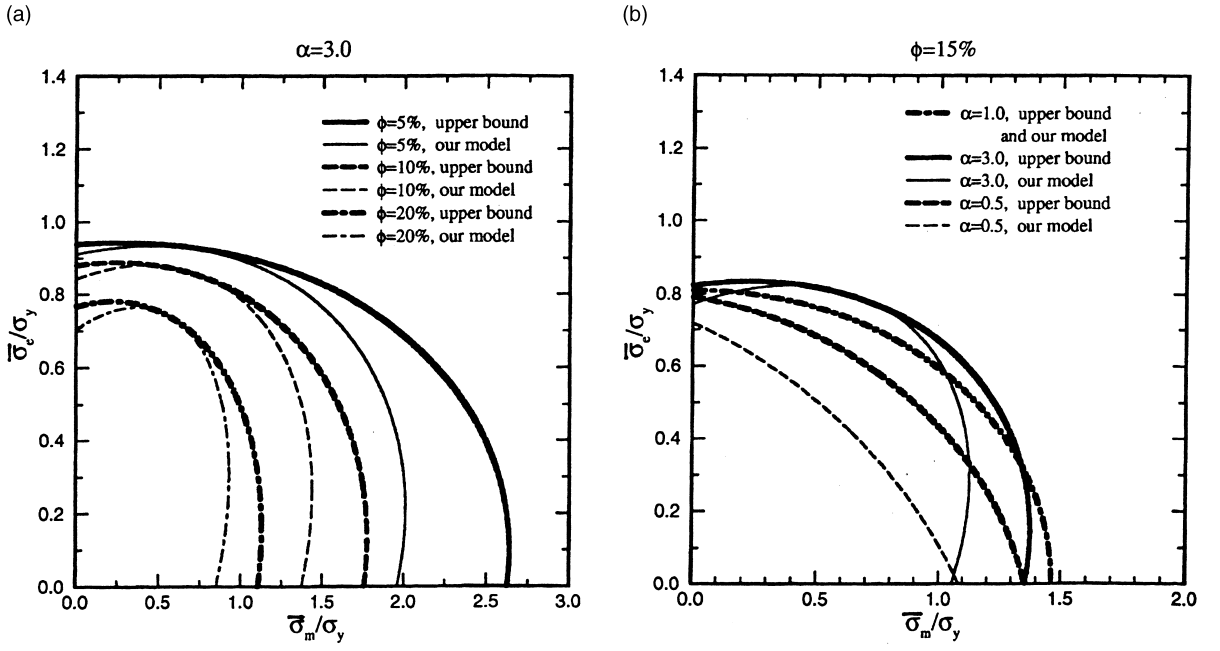

Fig. 12. Comparisons with upper bounds for ductile materials with different (a) volume fractions and (b) aspect ratios of aligned spheroidal voids.

the yield surface shrinks inwards as the porosity ϕ increases. It is emphasized that the present yield surface recovers exactly the upper bound when voids become spherical, as proved by Ju and Tseng (1996). Again, from Fig. 12(b), we notice that the present predictions are inside the corresponding upper bounds.

6. Elasto-viscoplastic behavior of PRMMCs

The proposed effective elastoplasticity formulation for PRMMCs can be easily extended to accommodate the rate-dependent viscoplasticity effect. Here, the viscoplastic model proposed by Duvaut and Lions (1972) is employed. For the present isotropic hardening elastoplastic model, the corresponding rate equations for Duvaut–Lions viscoplasticity are

$$\dot{\bar{\boldsymbol{\epsilon}}}^{\mathrm{vp}} = \frac{1}{\eta}\mathbf{C}^{*-1} : (\bar{\boldsymbol{\sigma}} - \bar{\bar{\boldsymbol{\sigma}}}), \tag{44}$$

$$\dot{\bar{e}}^{\mathrm{vp}} = -\frac{1}{\eta}(\bar{e}^{\mathrm{vp}} - \bar{\bar{e}}^{\mathrm{p}}), \tag{45}$$

where η is a viscosity coefficient and $\mathbf{C}^*$ is the effective elasticity tensor as defined in Eq. (66) of Ju and Sun (2000); and $\bar{\bar{\boldsymbol{\sigma}}}$ and $\bar{\bar{e}}^{\mathrm{p}}$ denote the stress tensor and hardening parameter, respectively, of the solution from the inviscid elastoplastic problem. Moreover, $\dot{\bar{\boldsymbol{\epsilon}}}^{\mathrm{vp}}$, $\bar{\boldsymbol{\sigma}}$ and $\dot{\bar{e}}^{\mathrm{vp}}$ signify the viscoplastic strain rate tensor, the total stress tensor and the rate of the hardening parameter $\bar{e}^{\mathrm{vp}}$, respectively.

Following Ju (1990) and Ju and Tseng (1997), the backward Euler discrete formulation of Eqs. (44) and (45) can be expressed as

$$\bar{\boldsymbol{\sigma}}_{n+1} = \frac{1}{1+\frac{\Delta t_{n+1}}{\eta}}\left[\bar{\boldsymbol{\sigma}}_n + \mathbf{C}^* : \Delta\bar{\epsilon}_{n+1} + \frac{\Delta t_{n+1}}{\eta}\bar{\bar{\boldsymbol{\sigma}}}_{n+1}\right], \tag{46}$$

$$\bar{e}^{\mathrm{vp}}_{n+1} = \frac{1}{1+\frac{\Delta t_{n+1}}{\eta}}\left[\bar{e}^{\mathrm{vp}}_n + \frac{\Delta t_{n+1}}{\eta}\bar{\bar{e}}^{\mathrm{p}}_{n+1}\right], \tag{47}$$

where Δt_{n+1} is the $(n+1)$th time step and $\Delta\bar{e}_{n+1}$ is the overall total strain increment.

Fig. 13(a)–(c) renders the overall elasto-viscoplastic behavior of PRMMCs under uniaxial tension. It is shown in Fig. 13(a) that the overall responses of the Duvaut–Lion viscoplasticity lie between the elastic predictor ($\eta \to \infty$) and the inviscid plasticity solution ($\eta \to 0$). In addition, Fig. 13(b) illustrates that the viscoplastic behavior becomes more effective when the volume fraction of particles increases. From Fig. 13(c), we notice that the effect of reinforcement shape on the elasto-viscoplastic behavior of PRMMCs is significant. In particular, prolate and oblate spheroidal particles are the most and the least effective, respectively, in strengthening the elasto-viscoplastic responses.

7. Conclusions

Emanating from the framework proposed by Ju and Sun (2000), effective elastoplastic constitutive formulations are applied to various loading conditions for two-phase metal matrix composites containing unidirectionally aligned and randomly located spheroidal inhomogeneities. We start by studying the uniaxial elastoplastic stress–strain behavior of PRMMCs. Comparisons are performed among our theoretical uniaxial predictions, experimental data of SiC/Al composites and existing finite element simulations to demonstrate the potential of the proposed framework. The effect of stress triaxiality is subsequently explored under either the purely hydrostatic or axisymmetric loading upon the overall elastoplastic responses of PRMMCs. In addition, the proposed initial effective yield surfaces for PRMMCs are simulated and

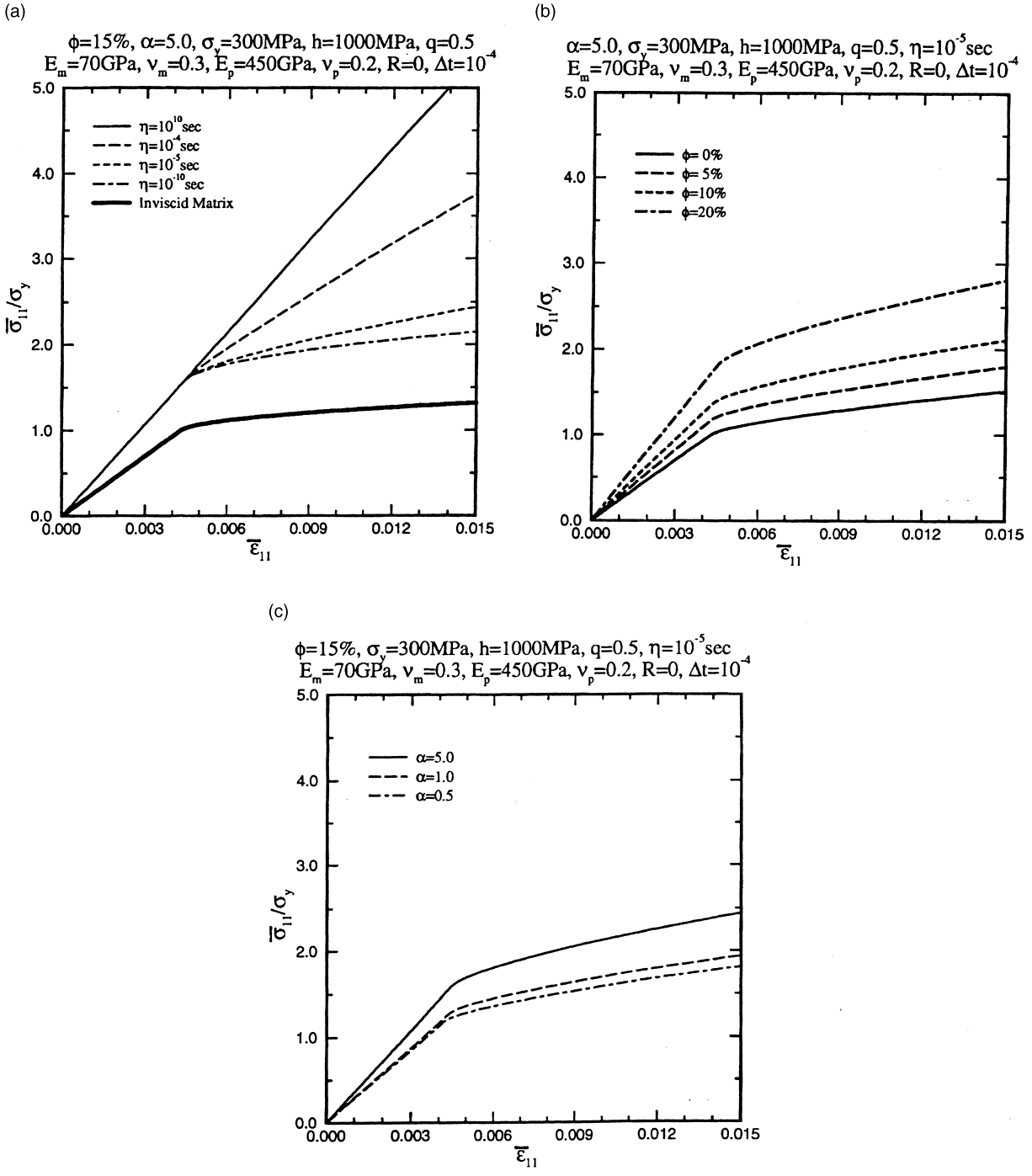

Fig. 13. Effects of (a) viscosity coefficients, (b) volume fractions of particles, and (c) aspect ratios of particles on the normalized uniaxial elasto-viscoplastic behavior of PRMMCs.

compared with the corresponding results from experiments. The initial effective yield criterion for incompressible ductile matrix containing aligned spheroidal voids is investigated and compared with the mathematical upper bound. The extension to viscoplasticity is also briefly discussed.

The proposed framework is capable of handling three-dimensional loading and unloading conditions. Therefore, the proposed constitutive equations are promising for the analyses and computations of structural components and systems made of PRMMCs. However, care should be taken in terms of the range of the aspect ratio and particle volume fraction in connection with the proposed model. Specifically, we should avoid extreme values of the aspect ratio and particle volume fraction.

Acknowledgements

This work was sponsored by the National Science Foundation, Mechanics and Materials Program, under the PYI Grant MSS-9157238. This support is gratefully acknowledged, In addition, the authors are grateful for the very helpful comments provided by two reviewers.

References

Bao, G., Hutchinson, J.W., McMeeking, R.M., 1991. Particle reinforcement of ductile matrices against plastic flow and creep. Acta Metall. Mater. 39, 1871–1882.

Christman, T., Needleman, A., Nutt, S., Suresh, S., 1989a. On microstructural evolution and micromechanical modelling of deformation of a whisker-reinforced metal-matrix composite. Mater. Sci. Engng. A107, 49–61.

Christman, T., Needleman, A., Suresh, S., 1989b. An experimental and numerical study of deformation in metal–ceramic composites. Acta Metall. 37, 3029–3050.

Drucker, D.C. 1951. A more fundamental approach to plastic stress–strain relations. Proceedings of the First US National Congress in Applied Mechanics. ASME, New York, pp. 487–491.

Drucker, D.C., 1959. A definition of stable inelastic material. J. Appl. Mech. ASME 26, 101–106.

Duvaut, G., Lions, J.L., 1972. Les inequations en mechanique et physique (in French).

Eshelby, J.D., 1957. The determination of the elastic field of an ellipsoidal inclusion, and related problems. Proc. R. Soc. Lond. A241, 376–396.

Eshelby, J.D., 1959. The elastic field outside an ellipsoidal inclusion. Proc. R. Soc. Lond. A252, 561–569.

Eshelby, J.D., 1961. Elastic inclusions and inhomogeneities In: Sneddon, I.N., Hill, R. (Eds.), Progress in Solid Mechanics, vol. II. North-Holland, Amsterdam, pp. 87–140.

Hom, C.L., 1992. Three-dimensional finite element analysis of plastic deformation in a whisker-reinforced metal matrix composite. J. Mech. Phys. Solids 40, 991–1008.

Ju, J.W., 1990. Consistent tangent moduli for a class of viscoplasticity. J. Engng. Mech. ASCE 116, 1764–1779.

Ju, J.W., Lee, H.K., 2000. A micromechanical damage model for effective elastoplastic behavior of ductile matrix composites considering evolutionary complete particle debonding. Computer Meth. Appl. Mech. Engng. 183, 201–222.

Ju J.W., Sun, L.Z., 2000. Effective elastoplastic behavior of metal matrix composites containing randomly located aligned spheroidal inhomogeneities, Part I: micromechanics-based formulation. Int. J. Solids Struct. 38, 183–201.

Ju, J.W., Tseng, K.H., 1996. Effective elastoplastic behavior of two-phase ductile matrix composites: a micromechanical framework. Int. J. Solids Struct. 33, 4267–4291.

Ju, J.W., Tseng, K.H., 1997. Effective elastoplastic algorithms for ductile matrix composites. J. Engng. Mech. ASCE 123, 260–266.

Lee, B.J., Mear, M.E., 1991. Effect of inclusion shape on the stiffness of nonlinear two-phase composites. J. Mech. Phys. Solids 39, 627–649.

Levy, A., Papazian, J.M., 1990. Tensile properties of short fiber-reinforced SiC/Al composites, Part II: finite-element analysis. Metall. Trans. A 21A, 411–420.

Levy, A., Papazian, J.M., 1991. Elastoplastic finite element analysis of short-fiber-reinforced SiC/Al composites: effect of thermal treatment. Acta Metall. Mater. 39, 2255–2266.

Li, G., 1992. Constitutive models for ductile solids reinforced by spheroidal inclusions. Ph.D. Thesis. Johns Hopkins University, Baltimore, MD, USA.

Li, G., Castaneda, P.P., 1994. Variational estimates for the elastoplastic response of particle-reinforced metal–matrix composites. Appl. Mech. Rev. 47, S77–S94.

Lynch, J.F., Ruderer, C.G., Duckworth, W.H., 1966. Engineering Properties of Selected Ceramic Materials. The American Ceramic Society, Columbus, OH, USA.

Mura, T., 1987. Micromechanics of Defects in Solids, second edn. Martinus Nijhoff.

Papazian, J.M., Adler, P.N., 1990. Tensile properties of short fiber-reinforced SiC/Al composites, Part I: effect of matrix precipitates. Metall. Trans. A 21A, 401–410.

Castaneda, P.P., 1991. The effective mechanical properties of nonlinear isotropic composites. J. Mech. Phys. Solids 39, 45–71.

Povirk, G.L., Needleman, A., Nutt, S.R., 1991. An analysis of the effect of residual stresses on deformation and damage mechanisms in Al–SiC composites. Mater. Sci. Engng. A132, 31–38.

Qiu, Y.P., Weng, G.J., 1992. A theory of plasticity for porous materials and particle reinforced composites. J. Appl. Mech. ASME 59, 261–268.

Qiu, Y.P., Weng, G.J., 1993. Plastic potential and yield function of porous materials with aligned and randomly oriented spheroidal voids. Int. J. Plasticity 9, 271–290.

Qiu, Y.P., Weng, G.J., 1995. An energy approach to the plasticity of a two-phase composite containing aligned inclusions. J. Appl. Mech. ASME 62, 1039–1046.

Tvergaard, V., 1990. Analysis of tensile properties for a whisker-reinforced metal-matrix composite. Acta Metall. Mater. 38, 185–194.

Voyiadjis, G.Z., Thiagarajan, G., 1995. An anisotropic yield surface model for directionally reinforced metal-matrix composites. Int. J. Plasticity 11, 867–894.

Zahl, D.B., McMeeking, R.M., 1991. The influence of residual stress on the yielding of metal matrix composites. Acta Metall. Mater. 39, 1117–1122.

Zhu, H.T., Zbib, H.M., Khraisheh, M.K., 1995. Flow strength and size effect of an Al–Si–Mg composite model system under multiaxial loadings. Scripta Metall. Mater. 32, 1895–1902.